ACS Catalysis

Research Article

pubs.acs.org/acscatalysis

Electrode-Ligand Interactions Dramatically Enhance CO_2 Conversion to CO by the [Ni(cyclam)]$(PF_6)_2$ Catalyst

Yueshen Wu,[†,‡,⊥] Benjamin Rudshteyn,[†,‡,⊥] Almagul Zhanaidarova,[§] Jesse D. Froehlich,[§] Wendu Ding,[†,‡,∥] Clifford P. Kubiak,*[,§] and Victor S. Batista*[,†,‡]

[†]Department of Chemistry, Yale University, P.O. Box 208107, New Haven, Connecticut 06520, United States

[‡]Energy Sciences Institute, Yale University, P.O. Box 27394, West Haven, Connecticut 06516, United States

[§]Department of Chemistry and Biochemistry, University of California, San Diego, 9500 Gilman Drive, MC 0358, La Jolla, California 92093, United States

Supporting Information

ABSTRACT: Dramatic enhancement of electrochemical CO_2 conversion to CO, catalyzed by [Ni(cyclam)]$(PF_6)_2$ is observed on mercury/gold electrodes. We find that Hg provides favorable noncovalent dispersive interactions with the cyclam ligand. As a result, the Hg surface destabilizes the poisoned CO-bound form of the catalyst, leading to enhanced reaction kinetics. These findings are particularly relevant to the design of ligands that improve the electrocatalytic performance of transition-metal complexes on interaction with metallic surfaces under cell operating conditions.

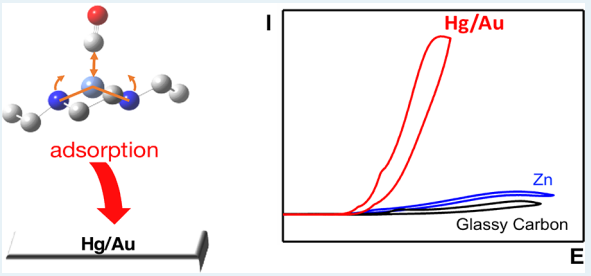

KEYWORDS: *CO_2 electroreduction, adsorption, CO poisoning, dispersive interaction, nickel cyclam*

INTRODUCTION

Electrochemical conversion of carbon dioxide (CO_2) to energy-dense fuels could lower the current dependence on fossil fuels by providing alternatives to petroleum-based feedstocks.[1−4] We focus on CO_2 conversion to carbon monoxide (CO):

$$CO_2 + 2H^+ + 2e^- \rightarrow H_2O + CO$$

CO could be subsequently converted into hydrocarbon fuels by the Fischer−Tropsch reaction:

$$(2n + 1)H_2 + nCO \rightarrow C_nH_{2n+2} + nH_2O$$

Reduction of CO_2 on metal surfaces usually requires considerably negative potentials and yields a wide range of products due to competing processes. In addition, the electrodes suffer from being poisoned by intermediates and/or products from competing reactions.[5,6] In contrast, molecular homogeneous catalysts can enhance selectivity toward CO.[7,8]

Many different molecular catalysts have been explored for CO_2 reduction.[9−12] However, it is rare to find catalysts based on earth-abundant metals exhibiting high selectivity, efficiency, and turnover frequencies. Some notable catalysts containing first-row transition metals (Mn, Fe, Co, Ni) have been reported.[9,13−15] However, the effectiveness of homogeneous catalysts is typically compromised when they are tethered to an electrode surface.[16,17] A remarkable exception is [Ni(cyclam)]$^{2+}$ (cyclam = 1,4,8,11-tetraazacyclotetradecane) and its derivatives, which exhibits a dramatic enhancement of turnover frequencies in contact with Hg electrode surfaces.[12,18−22] When it is operated in homogeneous aqueous solution, the catalyst is proposed to reduce CO_2 through the mechanism in Scheme 1,[19,23,24] where [Ni(cyclam)]$^{2+}$ gets electrochemically reduced to [Ni(cyclam)]$^+$ in the first step. The Hg surface adsorbs the catalytically active state of [Ni(cyclam)]$^+$,[19,25] where the enhanced CO_2 reduction takes place.[26,27] Therefore, it is of great interest to analyze how the surface affects the stability of key intermediates and kinetically favors the reaction while

Scheme 1. Catalytic Cycle for CO_2 Reduction by [Ni(cyclam)]$^{2+}$ and Deactivation by CO Poisoning[a]

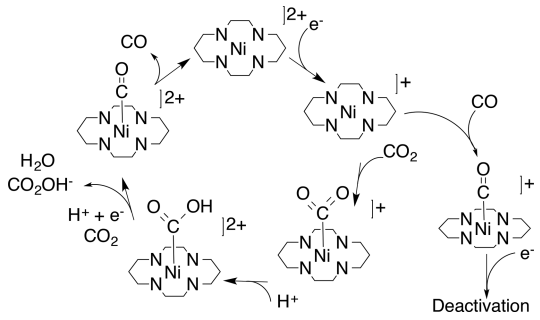

[a]The hydrogen atoms on secondary amine groups around Ni centers are omitted for clarity.

Received: April 4, 2017
Revised: June 21, 2017
Published: June 29, 2017

DOI: 10.1021/acscatal.7b01109
ACS Catal. 2017, 7, 5282−5288

serving as a mediator between the CO_2 substrate and the ultimate source of reducing equivalents.

CO poisoning is the major limitation to greater catalytic currents in the homogeneous phase, where CO desorption is rate-limiting.[28] Due to the enhanced rates on mercury/gold amalgam electrodes (abbreviated as Hg/Au, which is effectively an adlayer of Hg on an Au substrate) in comparison to other electrodes, it was proposed that Hg might suppress CO poisoning and deactivation of the active catalyst, as shown in Scheme 1. However, the origin of the enhanced rate remains to be elucidated at the molecular level. Here, we focus on the thermodynamics and kinetics of rate-limiting CO binding to the reactive intermediate $[Ni(cyclam)]^+$ adsorbed on Hg surfaces, in comparison to binding to the complex bound to a Zn electrode surface, since Zn is in the same group (12) in the periodic table. Additionally, it has been studied for CO_2 electroreduction on its own.[29]

We find that the origin of the kinetic enhancement is 2-fold: (1) Hg selectively adsorbs the more active *trans*-III conformer of $[Ni(cyclam)]^+$ through dispersive interactions and (2) Hg induces flattening of the cyclam ligand, which in turn facilitates CO desorption, the turnover-limiting step of the catalytic cycle.[28] For comparison, we analyze CO binding to $[Ni(cyclam)]^+$ on a Zn surface and to the free $[Ni(cyclam)]^+$ and find that the adsorption of $[Ni(cyclam)]^+$ and $[Ni(cyclam)(CO)]^+$ on Zn is much weaker than that on Hg. Structural changes of $[Ni(cyclam)(CO)]^+$ upon adsorption onto Zn are minimal, leading to similar electrocatalytic activity using a Zn electrode or a glassy-carbon electrode. Our study illustrates the subtle, but active, role played by the Hg electrode surface through London dispersion (noncovalent interactions) and provides an insightful example to the often-overlooked effects of dispersive interactions on catalysis.[30,31]

EXPERIMENTAL SECTION

Cyclic voltammetry experiments were performed using a BASi Epsilon potentiostat and a Gamry Reference 600 potentiostat. Tetrabutylammonium hexafluorophosphate ($TBAPF_6$, 0.1 M) was used as the electrolyte. A one-compartment cell was used with a Pt-wire counter electrode and a Ag wire with a Vycor frit as a reference electrode. Three types of working electrodes were used: glassy-carbon electrode (3 mm diameter from BASi), Zn wire (1 mm diameter × 5 mm length), and the Hg/Au amalgam electrode. The Zn electrode was polished using a 1800 fine grid polishing pad between each CV scan and was subjected to a negative potential (−1.4 V vs NHE) before the electrochemical measurements (Figure S1A in the Supporting Information). The Hg/Au amalgam electrode was prepared by dipping a 1.6 mm diameter Au-disk electrode (BASi) into a pool of mercury. The scan rate was 0.1 V/s. The surface area of the electrode was similar to that of the drop in the hanging mercury drop electrode (HDME) used in previous work.[27]

All cyclic voltammogram potentials were converted to the normal hydrogen electrode (NHE) reference by adding 0.54 V.[28] For the temperature-dependent peak current experiment, an electrochemical cell with the Hg/Au electrode in a methanol solution of 0.1 M LiCl and 1 mM of $[Ni(cyclam)](PF_6)_2$ under CO_2 in a dry ice/acetone bath was used that was warmed slowly. Methanol was used for this study, because it has a freezing point (−97.6 °C) lower than that of Hg (−39 °C) and is itself a proton source. The temperature was monitored with a probe placed next to the Hg/Au electrode.

The cyclic voltammogram of $[Ni(cyclam)](PF_6)_2$ on Zn does not show significant catalytic current for the CO_2 reductive wave (the increase in current beyond −1.6 V vs NHE is due to the solvent window).

The proton reduction peak has the same intensity near −1.3 V vs NHE regardless of whether the atmosphere is sparged with N_2 or CO_2. This assignment is also supported by the increase in current upon the addition of water (Figure 1 and Figure S1D in the Supporting Information). Proton reduction is corroborated by the large amounts of hydrogen produced by the blank Zn electrode in the controlled potential experiment as shown in Table S1, section S1, in the Supporting Information.

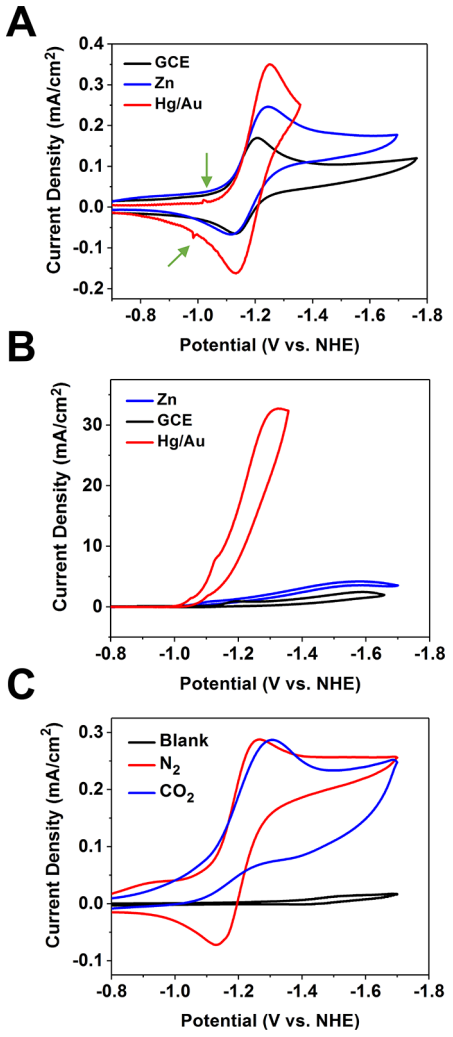

Figure 1. Cyclic voltammograms of 1 mM $[Ni(cyclam)](PF_6)_2$ with 0.1 M tetrabutylammonium hexafluorophosphate (A) under N_2 in dry acetonitrile on a GCE (black), Zn working electrode (blue), and Hg/Au electrode (red; green arrows point to the prewaves indicating adsorption), (B) under CO_2 with 20% water added, (C) on a Zn electrode under N_2 (red), under CO_2 (blue), and with a blank solution without $[Ni(cyclam)](PF_6)_2$ under N_2 (black). The cathodic current is indicated as positive.

These results preclude the formation of ZnO and electrocatalytic reduction of CO_2 within the solvent window. The GCE potential shift under CO_2, as in Figure S1B,C in the Supporting Information, is indicative of CO_2 binding to $[Ni(cyclam)]^{2+}$.

DOI: 10.1021/acscatal.7b01109
ACS Catal. 2017, 7, 5282−5288

COMPUTATIONAL METHODS

Metal surfaces are modeled as single-layer sheets consisting of 16 atoms. The sheets were prepared using the crystallographic structure of rhombohedral Hg[32] and *hcp* Zn.[33] Thye rhombohedral mercury (100) surface from α-phase solid Hg has been shown to represent well the properties of liquid mercury[34] and has been modeled before to study water adsorption on Hg.[35,36] For Zn, both Zn(101) and Zn(002) facets were found to be dominant facets in Zn foils[37] and have been modeled in a previous study.[37] The optimized geometries and adsorption energies of relevant adsorbates on Zn(101) are very similar to those on Zn(002) (see section 5 in the Supporting Information). The Zn(002) facet is investigated in details in our study.

DFT geometry optimization calculations were performed by using the hybrid functional ωB97XD,[38,39] as implemented in Gaussian 09 (Rev. D.01).[40] The Grimme D2 dispersion model is contained in the functional to quantify dispersive interaction as a correction term to the energy of the system.[41,42] The basis set included LANL2TZ[43−46] pseudopotential for metals and 6-31G(d)[47] for nonmetals. The solvent correction is implemented using the SMD model[48] to account for the difference in solvation energy resulting from the difference in geometries of the molecules before and after adsorption to the surface. The metal surface is not solvated and therefore is not included in the solvation model.[49−51] Details on solvent calculations are included in section 2 in the Supporting Information. Hg or Zn atoms were constrained to preserve the geometry of the slab. The frequency calculations did not include unrelaxed atoms and exhibited no imaginary frequencies. The CO stretching frequency is rescaled by a factor of 0.949, as recommended for a similar basis set by the Computational Chemistry Comparison and Benchmark DataBase (CCCBDB).[52] The Ni(I) redox state was confirmed through spin population analysis, which indicated a spin population on Ni between 0.88 and 0.94 (Table S3 in the Supporting Information), close to the formal value of 1. The details of this approach are given in section 2 in the Supporting Information. Spin contaminations are corrected using an established approach (section 3 in the Supporting Information). Structures were confirmed to have no internal instabilities via the use of the "stable = opt" keyword.[53−55]

Relaxed energy scans were used to probe the kinetics of adsorption and desorption of CO. Free energies of adsorption and electronic CO binding energies were calculated according to Scheme 2. Counterpoise calculations were performed to correct for basis set superposition error (BSSE) in adsorption energy.[56,57]

Scheme 2. Thermodynamic Cycle Used in This Study To Calculate the Free Energy of Adsorption of $[Ni(cyclam)]^+$ (ΔG_2) and $[Ni(cyclam)CO]^+$ (ΔG_1) on a Surface (M = Hg, Zn) and the CO Binding Free Energy of Free $[Ni(cyclam)]^+$ (ΔG_3) and Surface-Bound $[Ni(cyclam)]^+$ (ΔG_4)

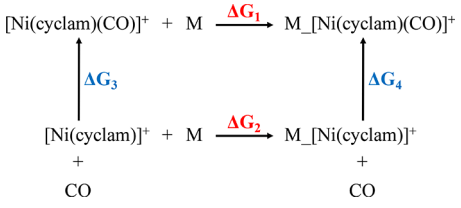

RESULTS AND DISCUSSION

Experimental Comparison of Hg/Au, Zn, and Glassy-Carbon Electrodes. Figure 1A shows the cyclic voltammogram (CV) of $[Ni(cyclam)](PF_6)_2$ in dry acetonitrile, using an Hg/Au amalgam electrode, Zn electrode, and glassy carbon working electrode (GCE). A small prewave can be seen on the CV near −1.0 V using the Hg/Au electrode, which is recognized as a distinctive signature of adsorption of $[Ni(cyclam)]^{2+}$ on the electrode.[19,25] Catalytic current was observed with $[Ni(cyclam)]^{2+}$ on an Hg/Au electrode under CO_2 in the presence of water as a proton source. To show the special effect of Hg on the catalytic activity of $[Ni(cyclam)]^+$, the same experiment was performed with a Zn working electrode, as Zn is in the same group as Hg. No catalytic activity was observed in the system for a Zn electrode without a proton source (Figure 1C). Although catalytic current was detected in the presence of water, this current was almost 10 times lower than that on Hg/Au amalgam (Figure 1B). Similar catalytic activity was observed with $[Ni(cyclam)]^{2+}$ on a glassy-carbon electrode (GCE) in acetonitrile in the presence of water and was not observed in dry acetonitrile without a proton source (Figure S1 in the Supporting Information).[28] Additionally, via a controlled-potential experiment, Table S2 in the Supporting Information shows that the turnover frequency (TOF) and turnover number (TON) (2.27 h^{-1} and 0.65, respectively) are even smaller than those for the GCE (4.18 h^{-1} and 1.19, respectively). The TOF and TON values are 2 orders of magnitude smaller than those obtained using HDME (32 h^{-1} and 116, respectively).[27] It should be noted that, for the experiment performed in dry acetonitrile, hydrogen generation was limited and was not the reason for low CO_2 conversion.

The most obvious difference between Hg and other transition metals is that Hg is liquid at room temperature—i.e., relevant experimental conditions. Therefore, we explored whether the liquid state could allow for interactions between $[Ni(cyclam)]^+$ and Hg due to disordered conformers which do not exist on other metal surfaces. In addition, the constant renewal of the liquid Hg drop electrode could refresh the catalytic reaction center and suppress poisoning of the electrode surface. Although an Hg/Au amalgam working electrode was used to obtain the CV in Figure 1A, it is unclear whether the mercury layer covering the gold electrode is solid or at least partially liquid. To analyze if the liquid state of Hg has a significant effect on catalysis, an experiment was performed to determine whether there is an abrupt change in catalytic activity at around the melting point of Hg (−39 °C, 1 atm), as described in the Experimental Section.

CVs were taken at multiple temperatures, and the peak catalytic current was plotted against temperature (Figure 2). As expected, the catalytic current increases with temperature due to increased kinetics of the electrochemical and electron transfer processes. However, there is no abrupt increase as the temperature crosses the melting point of Hg. Since no abrupt change was observed at that temperature, we conclude that the liquid state is not the main reason for the special properties of Hg with adsorbed $[Ni(cyclam)]^+$, with regard to the electrocatalytic reduction of CO_2.

Active Conformer on Hg Electrode. In aqueous solution two different conformers of $Ni(cyclam)^{2+}$, *trans*-I and *trans*-III, exist respectively in a 15% and 85% equilibrium.[58] There is a lack of consensus in the literature on the active conformer of $[Ni(cyclam)]^+$ and which conformer is adsorbed on the Hg

DOI: 10.1021/acscatal.7b01109
ACS Catal. 2017, 7, 5282−5288

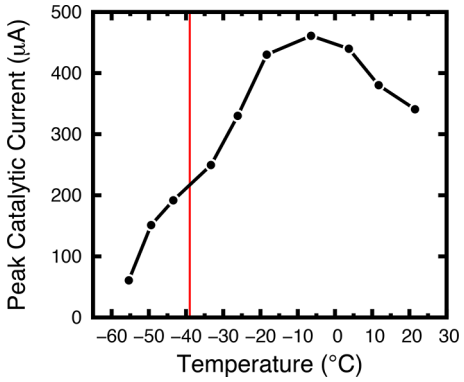

Figure 2. Peak catalytic current vs temperature of CV of 1 mM $[Ni(cyclam)](PF_6)_2$ with 0.1 M LiCl in methanol on an Hg/Au working electrode. The position of the red line indicates the melting point of Hg (−39 °C, 1 atm).

electrode, given that isomerization could occur near the electrode surface.[21,25,59,60] Some studies pointed to the *trans*-I conformer as the active species, backed by DFT calculations which showed that *trans*-I $[Ni(cyclam)]^+$ binds to CO_2 more readily.[59,61] Recently, Kubiak and co-workers assigned CO desorption from the deactivated catalyst $Ni(cyclam)(CO)^+$ (a step that lies in the catalyst deactivation pathway) as the rate-limiting step. It was shown through DFT calculations that in the homogeneous case *trans*-III $[Ni(cyclam)]^+$ binds CO more weakly than *trans*-I conformer.[28] It is therefore important to determine which conformer is the active form on adsorption on an Hg electrode. Figure 3 and Figure S2 in the Supporting Information show the DFT-optimized conformers of both $[Ni(cyclam)]^+$ and $[Ni(cyclam)(CO)]^+$ when they are adsorbed on Hg. These conformers can be best distinguished by the number of N−H bonds pertaining to the cyclam ligand that point toward the Hg surface. The *trans*-I bowl has four

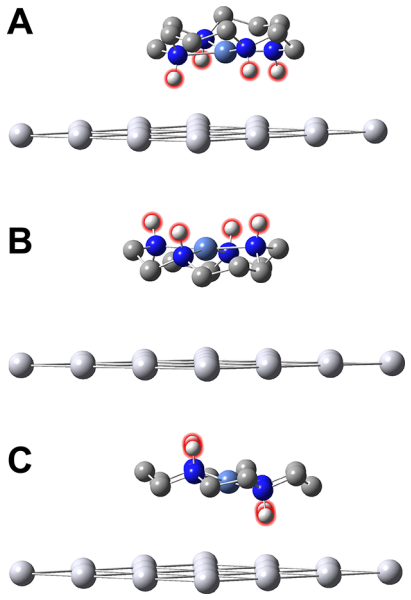

Figure 3. Optimized geometries of (A) *trans*-I cap, (B) *trans*-I bowl, and (C) *trans*-III $[Ni(cyclam)]^+$ on an Hg surface. Color key: silver, Hg; light blue, Ni; dark blue, N; dark gray, C; white, H. Hydrogens on amine groups are highlighted in red. The methylene hydrogens are omitted for clarity.

such bonds, while the *trans*-I cap and *trans*-III have zero and two, respectively. Table 1 summarizes the energy of the

Table 1. Relative Total Free Energies of Different Conformers Adsorbed on Hg as Well as Their Free Energies of Adsorption after BSSE and Solvent Corrections[a]

conformer on Hg	relative free energy (kcal/mol)[b]	free energy of adsorption (kcal/mol)
trans-I bowl	4.9	−20.3 (−23.9)
trans-I cap	5.2	−16.1 (−18.5)
trans-III	0.0	−24.0 (−27.2)

[a]Energies without either correction are shown in parentheses. [b]values are relative to *trans*-III.

respective systems relative to that of *trans*-III on Hg and the adsorption energies of different conformers onto Hg. Our calculations show that *trans*-III $[Ni(cyclam)]^+$ is more stable on the Hg surface than the other two conformers by 2.6 and 11.8 kcal/mol, respectively, and that adsorption of the *trans*-III conformer is stronger than that of the other two as well. The same trend applies to the poisoned catalyst $[Ni(cyclam)(CO)]^+$ (Table S4 in the Supporting Information). We thus conclude that *trans*-III $[Ni(cyclam)]^+$ is the dominant active form of the catalyst on an Hg electrode and will be the focus of this study.

Nature of Adsorption on Hg. To elucidate the mode of interaction between the catalyst and Hg surface, we calculated the optimized structure of the relevant species (1) on an Hg surface, (2) on a Zn surface, and (3) without a surface (Figure S3 in the Supporting Information). On the basis of our previous analyses, the most important species is the CO-poisoned form of *trans*-III $[Ni(cyclam)]^+$. Table 2 summarizes the energetics of adsorption of $[Ni(cyclam)]^+$ and $[Ni(cyclam)(CO)]^+$ on Hg and Zn.

Table 2. Free Energy of Adsorption of *trans*-III $[Ni(cyclam)]^+$ or $[Ni(cyclam)(CO)]^+$ on Hg and on Zn after BSSE and Solvent Corrections[a] and the Contribution of the Dispersion Term to Adsorption

system	free energy of adsorption (kcal/mol)	dispersion energy (kcal/mol)
$[Ni(cyclam)]^+$ on Hg	−24.0 (−27.2)	−41.4
$[Ni(cyclam)]^+$ on Zn	−9.0 (−15.6)	−19.2
$[Ni(cyclam)(CO)]^+$ on Hg	−21.1 (−24.4)	−40.5
$[Ni(cyclam)(CO)]^+$ on Zn	−10.1 (−16.2)	−18.9

[a]Energies without either correction are shown in parentheses.

The adsorption energies of $[Ni(cyclam)(CO)]^+$ and $[Ni(cyclam)]^+$ are larger on Hg than on Zn by 11.0 and 15.0 kcal/mol, respectively. $[Ni(cyclam)]^+$ adsorbs onto the Hg electrode at a negative potential, as manifested by a prewave on the cyclic voltammogram of the system.[19,25,61,62] Such a prewave is absent in the CV with a Zn electrode (Figure 1A, blue). These results and observations are strong indications that $[Ni(cyclam)]^+$ species do not get adsorbed as strongly onto a Zn electrode as they do onto an Hg electrode, even though Hg and Zn belong to the same group in the periodic table. The same trend is observed for *trans*-I bowl and *trans*-I cap conformers as well (Table S5 in the Supporting Information).

DOI: 10.1021/acscatal.7b01109
ACS Catal. 2017, 7, 5282−5288

The dispersion term is the major contribution to the adsorption energy (Table 2), suggesting that the most probable interaction mode between $[Ni(cyclam)]^+$ species and the Hg electrode surface is through dispersive interaction. Since such an interaction is inversely proportional to the sixth power of separation ($\sim R^{-6}$),[63] the hydrogen atoms on the cyclam ligand pointing toward the Hg are most likely to be the main contributors to the adsorption. The very different behaviors of Hg and Zn can be attributed to the fact that Hg has many more electrons than Zn that can significantly enhance the induced-dipole−induced-dipole interaction.

Facilitated CO Desorption by Hg Surface. CO desorption kinetics is simulated by lengthening the Ni−CO bond while letting other parts of the system (except the surface) relax to the energy minimum. Figure 4 shows the

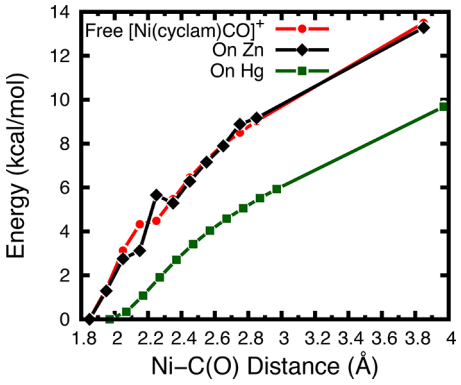

Figure 4. Electronic energy change versus Ni−CO distance during CO desorption for *trans*-III $[Ni(cyclam)(CO)]^+$ on Hg (green squares), on Zn (black diamonds), or by itself (red circles).

simulated CO desorption kinetics from *trans*-III $[Ni(cyclam)(CO)]^+$ (1) on Hg, (2) on Zn, and (3) by itself. Specifically, the electronic energies of the different structures with elongated Ni−CO bonds are plotted against Ni−CO distances. Notably, the Ni−CO bond length of the optimized $[Ni(cyclam)(CO)]^+$ is very close to that of a similar Ni macrocycle reported previously in an EXAFS study.[64] The simulated kinetics of CO desorption are very similar for $[Ni(cyclam)(CO)]^+$ adsorbed on Zn and by itself, as signified by the almost identical curvatures and values for the two cases, whereas *trans*-III $[Ni(cyclam)(CO)]^+$ shows a facilitated CO desorption kinetics on an Hg surface, indicated by the much smaller slope and the smaller energy value. On comparison across the systems where the Ni−CO distance is increased by 2.0 Å from the optimized structures, the energies of $[Ni(cyclam)(CO)]^+$ on Hg, on Zn, and free $[Ni(cyclam)(CO)]^+$ increase by 6.0, 9.2, and 9.2 kcal/mol, respectively.

The difference in CO desorption kinetics for *trans*-III $[Ni(cyclam)(CO)]^+$ in these three cases correlates well with the Ni−CO bond lengths and the average N−Ni−N bond angles of the respective systems (Scheme 3), as summarized in Table 3. In comparison to free $[Ni(cyclam)(CO)]^+$, the adsorbed form on Hg has a 0.12 Å longer Ni−CO bond, which is indicative of weaker CO binding to the Ni center. Such weakening of CO binding is associated with the geometric distortion from a more pyramidal NiN_4 unit to a more planar arrangement,[28,65] which is in line with the smaller N−Ni−N bond angle (greater deviation from linearity) when the complex is adsorbed on Hg. In other words, the Hg surface flattens the

Scheme 3. Geometric Parameters of *trans*-III $[Ni(cyclam)(CO)]^+$ Selected To Be Shown in Table 3[a]

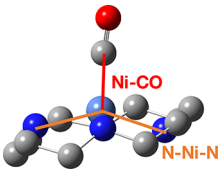

[a]Hydrogen atoms are omitted for clarity. Color key: light blue, Ni; dark gray, C; dark blue, N; red, O.

Table 3. CO Binding Affinities, Selected Bond Lengths, and Bond Angles of *trans*-III $[Ni(cyclam)(CO)]^+$ on Hg, on Zn, and on Its Own[a]

system	CO binding free energy (kcal/mol)	CO binding electronic energy (kcal/mol)	Ni−CO bond length (Å)	minimal N−Ni−N bond angle (deg)
$[Ni(cyclam)(CO)]^+$ on Hg	1.9	−8.4	1.97	164.8
$[Ni(cyclam)(CO)]^+$ on Zn	−2.1	−12.7	1.85	149.6
$[Ni(cyclam)(CO)]^+$	−2.8	−13.3	1.85	149.7

[a]Hydrogen atoms are omitted for clarity.

Ni macrocycle, which in turns significantly reduces the CO binding affinity.

Molecular Orbital Analysis of CO Binding. Figure 5 shows the orbitals relevant to CO binding and their energies for

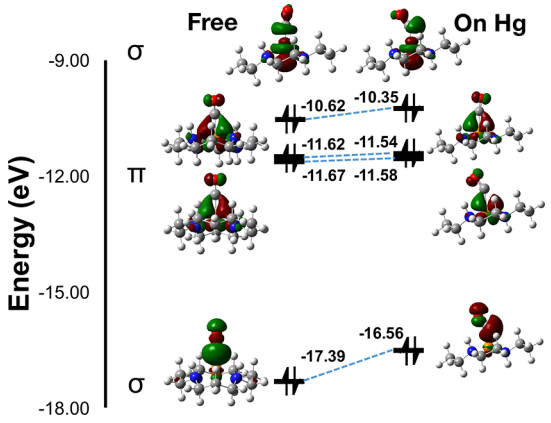

Figure 5. α molecular orbitals relevant to Ni−CO interactions in free *trans*-III $[Ni(cyclam)(CO)]^+$ and *trans*-III $[Ni(cyclam)(CO)]^+$ adsorbed on an Hg surface. Energy values reported here are the average values of α and β orbitals relative to vacuum. The Ni center is shown in orange for clarity.

both free $[Ni(cyclam)(CO)]^+$ and $[Ni(cyclam)(CO)]^+$ adsorbed on an Hg surface. The interaction between the Ni(I) center and the CO ligand can be dissected into σ donation from CO to Ni and π back-donation from Ni to CO. The σ interaction consists of a bonding orbital resulting from σ donation from CO to Ni (mostly localized on CO's lone pair) and a nonbonding orbital mostly localized on Ni. The π interaction consists of two bonding orbitals corresponding to π back donation from Ni to CO. After the complex adsorbs onto the surface, the most obvious changes in MOs occur in the σ-

DOI: 10.1021/acscatal.7b01109
ACS Catal. 2017, 7, 5282−5288

bonding regime; both σ-donation and σ-nonbonding orbitals are significantly destabilized, by 0.27 and 0.84 eV, respectively. This finding agrees with the longer Ni−C bond and the weaker CO binding energy of *trans*-III $[Ni(cyclam)(CO)]^+$ on an Hg surface, in comparison to its free form. On the other hand, the two orbitals associated with π back-donation are roughly unaffected in terms of their orbital energies. Notably, the CO stretching frequency, a direct indicator of the extent of π back-bonding, shifts to lower values for *trans*-III $[Ni(cyclam)(CO)]^+$ when it is surface-bound on Hg (Table S6 in the Supporting Information), which suggests that, although the Ni−CO bond is weakened on the Hg surface, the contribution of back-bonding to the overall Ni−CO interaction is greater when the complex is surface-bound. The CO stretching frequency therefore cannot be used as an indicator for the Ni−CO bond strength. The same conclusion was reached in a previous study by Gagne and co-workers.[66,67]

CONCLUSIONS

We have elucidated that ligand conformational changes account for the enhancement of electrochemical CO_2 to CO conversion on catalysis by $[Ni(cyclam)]^{2+}$ interacting with an Hg electrode. We find that Hg promotes adsorption of the *trans*-III conformer over *trans*-I. *trans*-III is the more active conformer of the catalyst, since it disfavors CO poisoning. We conclude that dispersive interactions induce flattening of the cyclam ligand, which in turn facilitates CO desorption kinetics by weakening Ni−CO σ interactions. These findings provide valuable insights for the design of molecular electrocatalysts on metallic surfaces with optimal reaction kinetics.

ASSOCIATED CONTENT

Supporting Information

and The Supporting Information is available free of charge on the ACS Publications website at DOI: 10.1021/acscatal.7b01109.

Experimental control cyclic voltammetry, controlled potential plots, TOF/TON data, Ni(I) spin densities, DFT optimized structures and energies for the *trans-I*-bowl and *trans-I*-cap conformers on Hg or Zn CO unscaled stretching frequencies, thermodynamic scheme, structures of solution-phase complexes, and discussion of the use of spin contamination corrections (PDF)

Cartesian coordinates/electronic energy for all structures in this study (PDF)

AUTHOR INFORMATION

Corresponding Authors

*E-mail for C.P.K.: ckubiak@ucsd.edu.

*E-mail for V.S.B.: victor.batista@yale.edu.

ORCID

Benjamin Rudshteyn: 0000-0002-9511-6780

Clifford P. Kubiak: 0000-0003-2186-488X

Victor S. Batista: 0000-0002-3262-1237

Present Address

[⊥]Department of Chemistry, Northwestern University, 2145 Sheridan Road, Evanston, IL 60208, USA.

Author Contributions

[‖]Y.W. and B.R. contributed equally.

Notes

The authors declare no competing financial interest.

ACKNOWLEDGMENTS

This research was funded by the Air Force Office of Scientific Research (AFOSR) through grant #FA9550-13-1-0020. B.R. acknowledges support from the National Science Foundation Graduate Research Fellowship under Grant No. DGE-1122492. V.S.B. acknowledges supercomputing time from the NERSC and from the Yale High Performance Computing Center. This work used the Extreme Science and Engineering Discovery Environment (XSEDE), which is supported by National Science Foundation grant number ACI-1053575. The authors thank Melissa L. Helm, Prof. Joshua S. Figueroa, and Prof. Tim Lian for helpful discussions.

REFERENCES

(1) Appel, A. M.; Bercaw, J. E.; Bocarsly, A. B.; Dobbek, H.; DuBois, D. L.; Dupuis, M.; Ferry, J. G.; Fujita, E.; Hille, R.; Kenis, P. J. A.; Kerfeld, C. A.; Morris, R. H.; Peden, C. H. F.; Portis, A. R.; Ragsdale, S. W.; Rauchfuss, T. B.; Reek, J. N. H.; Seefeldt, L. C.; Thauer, R. K.; Waldrop, G. L. *Chem. Rev.* **2013**, *113*, 6621−6658.

(2) Qiao, J.; Liu, Y.; Hong, F.; Zhang, J. *Chem. Soc. Rev.* **2014**, *43*, 631−675.

(3) Tu, W.; Zhou, Y.; Zou, Z. *Adv. Mater.* **2014**, *26*, 4607−4626.

(4) Berardi, S.; Drouet, S.; Francas, L.; Gimbert-Surinach, C.; Guttentag, M.; Richmond, C.; Stoll, T.; Llobet, A. *Chem. Soc. Rev.* **2014**, *43*, 7501−7519.

(5) Kedzierzawski, P.; Augustynski, J. *J. Electrochem. Soc.* **1994**, *141*, L58−L60.

(6) Jitaru, M.; Lowy, D. A.; Toma, M.; Toma, B. C.; Oniciu, L. *J. Appl. Electrochem.* **1997**, *27*, 875−889.

(7) Kumar, B.; Smieja, J. M.; Kubiak, C. P. *J. Phys. Chem. C* **2010**, *114*, 14220−14223.

(8) Kumar, B.; Llorente, M.; Froehlich, J.; Dang, T.; Sathrum, A.; Kubiak, C. P. *Annu. Rev. Phys. Chem.* **2012**, *63*, 541−569.

(9) Savéant, J.-M. *Chem. Rev.* **2008**, *108*, 2348−2378.

(10) Benson, E. E.; Kubiak, C. P.; Sathrum, A. J.; Smieja, J. M. *Chem. Soc. Rev.* **2009**, *38*, 89−99.

(11) Windle, C. D.; Perutz, R. N. *Coord. Chem. Rev.* **2012**, *256*, 2562−2570.

(12) Costentin, C.; Robert, M.; Saveant, J.-M. *Chem. Soc. Rev.* **2013**, *42*, 2423−2436.

(13) Bourrez, M.; Molton, F.; Chardon-Noblat, S.; Deronzier, A. *Angew. Chem., Int. Ed.* **2011**, *50*, 9903−9906.

(14) Costentin, C.; Drouet, S.; Robert, M.; Savéant, J.-M. *Science* **2012**, *338*, 90−94.

(15) Smieja, J. M.; Sampson, M. D.; Grice, K. A.; Benson, E. E.; Froehlich, J. D.; Kubiak, C. P. *Inorg. Chem.* **2013**, *52*, 2484−2491.

(16) Clark, M. L.; Rudshteyn, B.; Ge, A.; Chabolla, S. A.; Machan, C. W.; Psciuk, B. T.; Song, J.; Canzi, G.; Lian, T.; Batista, V. S. *J. Phys. Chem. C* **2016**, *120*, 1657−1665.

(17) Materna, K. L.; Rudshteyn, B.; Brennan, B. J.; Kane, M. H.; Bloomfield, A. J.; Huang, D. L.; Shopov, D. Y.; Batista, V. S.; Crabtree, R. H.; Brudvig, G. W. *ACS Catal.* **2016**, *6*, 5371−5377.

(18) Fisher, B. J.; Eisenberg, R. *J. Am. Chem. Soc.* **1980**, *102*, 7361−7363.

(19) Beley, M.; Collin, J. P.; Ruppert, R.; Sauvage, J. P. *J. Am. Chem. Soc.* **1986**, *108*, 7461−7467.

(20) Collin, J. P.; Sauvage, J. P. *Coord. Chem. Rev.* **1989**, *93*, 245−268.

(21) Schneider, J.; Jia, H.; Kobiro, K.; Cabelli, D. E.; Muckerman, J. T.; Fujita, E. *Energy Environ. Sci.* **2012**, *5*, 9502−9510.

(22) Fujita, E.; Haff, J.; Sanzenbacher, R.; Elias, H. *Inorg. Chem.* **1994**, *33*, 4627−4628.

(23) Kelly, C. A.; Blinn, E. L.; Camaioni, N.; D'Angelantonio, M.; Mulazzani, Q. G. *Inorg. Chem.* **1999**, *38*, 1579−1584.

(24) Kelly, C. A.; Mulazzani, Q. G.; Venturi, M.; Blinn, E. L.; Rodgers, M. A. *J. Am. Chem. Soc.* **1995**, *117*, 4911−4919.

(25) Balazs, G. B.; Anson, F. C. *J. Electroanal. Chem.* **1992**, *322*, 325−345.

DOI: 10.1021/acscatal.7b01109
ACS Catal. 2017, 7, 5282−5288

(26) Balazs, G. B.; Anson, F. C. *J. Electroanal. Chem.* **1993**, *361*, 149−157.
(27) Beley, M.; Collin, J.-P.; Ruppert, R.; Sauvage, J.-P. *J. Chem. Soc., Chem. Commun.* **1984**, 1315−1316.
(28) Froehlich, J. D.; Kubiak, C. P. *J. Am. Chem. Soc.* **2015**, *137*, 3565−3573.
(29) Hori, Y. In *Modern Aspects of Electrochemistry*; Vayenas, C. G., White, R. E., Gamboa-Aldeco, M. E., Eds.; Springer: New York, 2008; pp 89−189.
(30) Wagner, J. P.; Schreiner, P. R. *Angew. Chem., Int. Ed.* **2015**, *54*, 12274−12296.
(31) Miranda-Rojas, S.; Sierra-Rosales, P.; Muñoz-Castro, A.; Arratia-Pérez, R.; Zagal, J. H.; Mendizábal, F. *Phys. Chem. Chem. Phys.* **2016**, *18*, 29516−29525.
(32) Mehl, R.; Barrett, C. *Trans. AIME* **1930**, *89*, 575−588.
(33) Jette, E. R.; Foote, F. *J. Chem. Phys.* **1935**, *3*, 605−616.
(34) Bosio, L.; Cortes, R.; Segaud, C. *J. Chem. Phys.* **1979**, *71*, 3595−3600.
(35) Böcker, J.; Nazmutdinov, R. R.; Spohr, E.; Heinzinger, K. *Surf. Sci.* **1995**, *335*, 372−377.
(36) Böcker, J.; Gurskii, Z.; Heinzinger, K. *J. Phys. Chem.* **1996**, *100*, 14969−14977.
(37) Won, D. H.; Shin, H.; Koh, J.; Chung, J.; Lee, H. S.; Kim, H.; Woo, S. I. *Angew. Chem., Int. Ed.* **2016**, *55*, 9297−9300.
(38) Chai, J.-D.; Head-Gordon, M. *Phys. Chem. Chem. Phys.* **2008**, *10*, 6615−6620.
(39) Chai, J.-D.; Head-Gordon, M. *J. Chem. Phys.* **2008**, *128*, 084106.
(40) Frisch, M. J.; Trucks, G. W.; Schlegel, H. B.; Scuseria, G. E.; Robb, M. A.; Cheeseman, J. R.; Scalmani, G.; Barone, V.; Mennucci, B.; Petersson, G. A.; Nakatsuji, H.; Caricato, M.; Li, X.; Hratchian, H. P.; Izmaylov, A. F.; Bloino, J.; Zheng, G.; Sonnenberg, J. L.; Hada, M.; Ehara, M.; Toyota, K.; Fukuda, R.; Hasegawa, J.; Ishida, M.; Nakajima, T.; Honda, Y.; Kitao, O.; Nakai, H.; Vreven, T.; Montgomery, J. A., Jr.; Peralta, J. E.; Ogliaro, F.; Bearpark, M.; Heyd, J. J.; Brothers, E.; Kudin, K. N.; Staroverov, V. N.; Kobayashi, R.; Normand, J.; Raghavachari, K.; Rendell, A.; Burant, J. C.; Iyengar, S. S.; Tomasi, J.; Cossi, M.; Rega, N.; Millam, N. J.; Klene, M.; Knox, J. E.; Cross, J. B.; Bakken, V.; Adamo, C.; Jaramillo, J.; Gomperts, R.; Stratmann, R. E.; Yazyev, O.; Austin, A. J.; Cammi, R.; Pomelli, C.; Ochterski, J. W.; Martin, R. L.; Morokuma, K.; Zakrzewski, V. G.; Voth, G. A.; Salvador, P.; Dannenberg, J. J.; Dapprich, S.; Daniels, A. D.; Farkas, Ö.; Foresman, J. B.; Ortiz, J. V.; Cioslowski, J.; Fox, D. J. *Gaussian 09 Revision D.01*; Gaussian, Inc., Wallingford, CT, 2009.
(41) Grimme, S. *J. Chem. Phys.* **2006**, *124*, 034108.
(42) Grimme, S. *J. Comput. Chem.* **2006**, *27*, 1787−1799.
(43) Roy, L. E.; Hay, P. J.; Martin, R. L. *J. Chem. Theory Comput.* **2008**, *4*, 1029−1031.
(44) Wadt, W. R.; Hay, P. J. *J. Chem. Phys.* **1985**, *82*, 284−298.
(45) Hay, P. J.; Wadt, W. R. *J. Chem. Phys.* **1985**, *82*, 299−310.
(46) Hay, P. J.; Wadt, W. R. *J. Chem. Phys.* **1985**, *82*, 270−283.
(47) Hariharan, P. C.; Pople, J. A. *Theor. Chim. Acta* **1973**, *28*, 213−222.
(48) Marenich, A. V.; Cramer, C. J.; Truhlar, D. G. *J. Phys. Chem. B* **2009**, *113*, 6378−6396.
(49) Tripkovic, V.; Vanin, M.; Karamad, M.; Björketun, M. E.; Jacobsen, K. W.; Thygesen, K. S.; Rossmeisl, J. *J. Phys. Chem. C* **2013**, *117*, 9187−9195.
(50) Calle-Vallejo, F.; Krabbe, A.; Garcia-Lastra, J. M. *Chem. Sci.* **2017**, *8*, 124−130.
(51) Shen, J.; Kolb, M. J.; Gottle, A. J.; Koper, M. T. *J. Phys. Chem. C* **2016**, *120*, 15714−15721.
(52) Johnson, R. D., III In *NIST Standard Reference Database*, 2016.
(53) Schlegel, H. B.; McDouall, J. J. W. In *Computational Advances in Organic Chemistry: Molecular Structure and Reactivity*; Ögretir, C., Csizmadia, I., Eds.; Springer: Dordrecht, The Netherlands, 1991; Vol. *330*, pp 167−185.
(54) Seeger, R.; Pople, J. A. *J. Chem. Phys.* **1977**, *66*, 3045−3050.
(55) Bauernschmitt, R.; Ahlrichs, R. *J. Chem. Phys.* **1996**, *104*, 9047−9052.
(56) Simon, S.; Duran, M.; Dannenberg, J. J. *J. Chem. Phys.* **1996**, *105*, 11024−11031.
(57) Boys, S. F.; Bernardi, F. *Mol. Phys.* **1970**, *19*, 553−566.
(58) Connolly, P. J.; Billo, E. J. *Inorg. Chem.* **1987**, *26*, 3224−3226.
(59) Sakaki, S. *J. Am. Chem. Soc.* **1992**, *114*, 2055−2062.
(60) Froehlich, J. D.; Kubiak, C. P. *Inorg. Chem.* **2012**, *51*, 3932−3934.
(61) Schneider, J.; Jia, H.; Muckerman, J. T.; Fujita, E. *Chem. Soc. Rev.* **2012**, *41*, 2036−2051.
(62) Fujihira, M.; Hirata, Y.; Suga, K. *J. Electroanal. Chem. Interfacial Electrochem.* **1990**, *292*, 199−215.
(63) London, F. *Trans. Faraday Soc.* **1937**, *33*, 8b−26.
(64) Furenlid, L. R.; Renner, M. W.; Szalda, D. J.; Fujita, E. *J. Am. Chem. Soc.* **1991**, *113*, 883−892.
(65) Macgregor, S. A.; Lu, Z.; Eisenstein, O.; Crabtree, R. H. *Inorg. Chem.* **1994**, *33*, 3616−3618.
(66) Gagne, R. R.; Ingle, D. M. *J. Am. Chem. Soc.* **1980**, *102*, 1444−1446.
(67) Gagne, R. R.; Ingle, D. M. *Inorg. Chem.* **1981**, *20*, 420−425.

DOI: 10.1021/acscatal.7b01109
ACS Catal. 2017, 7, 5282−5288